World Model Based Sim2Real Transfer for Visual Navigation

Chen Liu*, Kiran Lekkala* and Laurent Itti†

***Abstract*— Sim2Real transfer has gained popularity because it helps transfer from inexpensive simulators to real world. This paper presents a novel system that fuses components in a traditional *World Model* into a robust system, trained entirely within a simulator, that *Zero-Shot* transfers to the real world. To facilitate transfer, we use an intermediary representation that are based on *Bird's Eye View (BEV)* images. Thus, our robot learns to navigate in a simulator by first learning to translate from complex *First-Person View (FPV)* based RGB images to BEV representations, then learning to navigate using those representations. Later, when tested in the real world, the robot uses the perception model that translates FPV-based RGB images to embeddings that are used by the downstream policy. The incorporation of state-checking modules using *Anchor images* and *Mixture Density LSTM* not only interpolates uncertain and missing observations but also enhances the robustness of the model when exposed to the real-world environment. We trained the model using data collected using a *Differential drive* robot in the CARLA simulator. Our methodology's effectiveness is shown through the deployment of trained models onto a *Real world Differential drive* robot. Lastly we release a comprehensive codebase, dataset and models for training and deployment that are available to the public.**

I. Introduction

[12]

Reinforcement Learning (RL) has predominantly been conducted in simulator environments, primarily due to the prohibitive costs associated with conducting trial-and-error processes in the real world. With the advances in graphics and computational technologies, there has been a significant development in realistic simulators that capture the system (robot) information. Due to these reasons, our model necessitates training within a simulator setting. However, the domain gap between synthetic and real data introduces a substantial performance drop when the models are directly deployed into real-world applications after training, a phenomenon commonly referred to as the *Sim2Real gap*.

Traditionally, Sim2real transfer methods either optimize training on a simulation that closely resembles real-world data, or use *Domain Randomization*[17] or *Domain Adaptation*[18]. Other works like [2] train on a simple simulated environment and deploy to self-driving cars. However, since these models were not trained in cluttered, pedestrian-rich environments, they would not generalize to some real-world

*Equal Contribution

[1] The authors are with Thomas Lord Department of Computer Science, University of Southern California, 90089, USA Correspondence to klekkala@usc.edu

This work was supported by C-BRIC (one of six centers in JUMP, a Semiconductor Research Corporation (SRC) program sponsored by DARPA) and the Army Research Office (W911NF2020053). The authors affirm that the views expressed herein are solely their own, and do not represent the views of the United States government or any agency thereof.

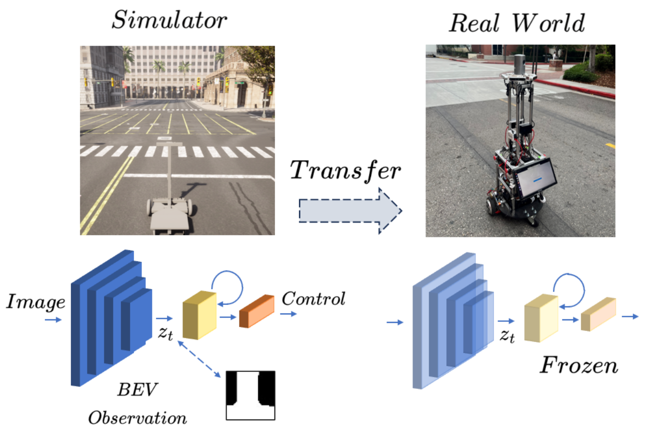

Fig. 1. **Overview of our system** We first train the visual navigation system on a large-scale dataset collected in the simulator and deploy the frozen model in an unseen real-world environment.

scenarios. Some of the recent works, such as [16] and [19], have shown promising results in attempting to cope with the Sim2real gap using *Style Transfer* but might not be suitable for visual navigation on drones and delivery robots which have limited computational bandwidth. With all these practical considerations, it is imperative that we design a robust method using low resource-footprint models that enables a mobile-robot to function in diverse scenarios.

In this paper, we formulate a new setting for *Zero-shot Sim2Real* transfer for *Visual Navigation without Maps*, involving data obtained from the CARLA simulator, as outlined in 1. We build a large dataset consisting of *First-person view (FPV)* and *Bird's eye view (BEV)* image sequences from the CARLA [3] simulator. The system is trained entirely on this simulated dataset and is frozen and deployed on a real-world mobile robot.

II. Related work

Traditional Sim2Real transfer methods for Visual Navigation comprise methods ranging from Fine-tuning[6], Meta-learning[1], GANs[16], Domain Randomization[14] to System Identification[7]. [14] proposes a method to train a model to perform collision-free flight entirely in the simulator and transfer it into the real world by domain randomization. [16] trains a Cycle-GAN to translate images taken from the simulator to the real-world. Although it is possible to predict a real-world image from a simulated image or vice-versa using style transfer, predicting representations would help the model remain lightweight and flexible, which is desirable for mobile platforms.

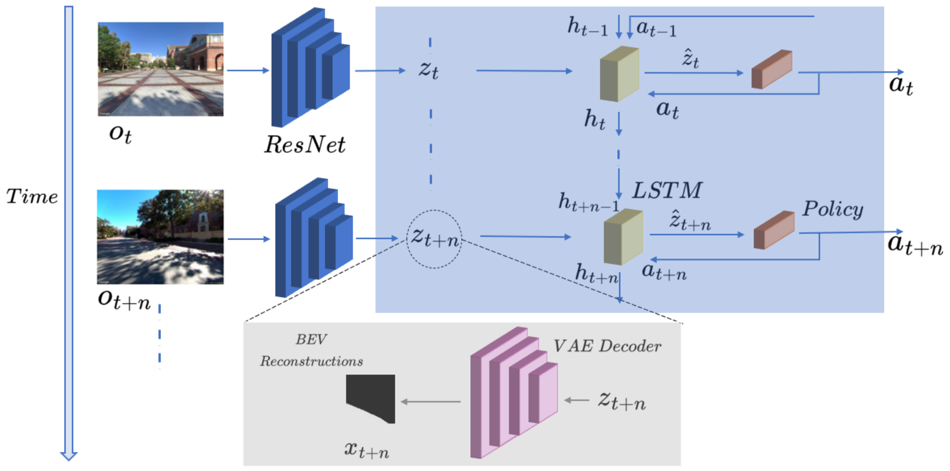

Fig. 2. **Working of the System** RGB observation o_t at time step t is passed to the ResNet-50 and compressed into a Bird's Eye View (BEV) based embedding z_t. The LSTM model takes the current latent representation and uses the historical context to refine the state into $\hat{z}_t$. The control policy takes the current state and gives a proper action command a_t. Blue box corresponds to the part of the system that sees the world only from a BEV based representation. Grey box depicts what would happen if we pass the output of the perception model into the VAE Decoder.

Bird's Eye View (BEV) based representation of a scene allows for a compact representation of the scene, invaraient to any texture changes, scene variations or lightning differences in an RGB image. This makes for an optimal representation for *PointGoal Navigation*. Some works estimate BEV semantic maps from RGB images, such as [9], [11] and [13]. However, semantic map prediction from FPV images often exhibits anomalies, showing that the FPV models proposed in prior methodologies are incapable of providing accurate BEV representations. Incorporating these intermediate predictions as inputs for training downstream models to ensure their compatibility, becomes a challenging task. In contrast, our approach enables downstream models to be trained entirely on ground truth BEV representations from the simulator while maintaining seamless compatibility with our FPV encoder. Furthermore, our primary focus resides in acquiring informative yet compact representations of monocular observations for the downstream task, therefore, pixel-wise segmentation from multiple camera views introduces unwarranted computational and calibration complexity. In addition, training on real-world datasets as [9] involves difficulty in obtaining real-world ground truth.

Recurrent world-models [4] introduces a novel approach to RL, incorporating a Vision model for sensory data representation and a Memory model for capturing temporal dynamics, all of which collectively improve agent performance. Apart from the advantages of pertaining each module, some of the modules in this architecture can be frozen after learning the representation of the environment, paving the way for more efficient and capable RL agents. In summary, the following are our contributions:

1) We propose a novel training regime and develop a Perception model that is trained on a large simulated dataset to translate FPV based RGB images into representations that align with the representations of the corresponding BEV images.
2) We upgrade the existing world models framework using a novel Model-based *Temporal State Checking (TSC)* and *Anchor State Checking (ASC)* methods that add robustness to the navigation pipeline when transferred to the real world.
3) We release 3 different codebases for pre-training, RL training and ROS based deployment of our system on a real-world robot. Along with the codebases, we also release a large FPV-BEV dataset and pre-trained models.

With the above contributions, we hope move closer towards open-sourcing a robust Visual Navigation system that uses models trained on large datasets and simulations for efficient representation learning.

III. Proposed Method

For an autonomous agent to navigate using camera imagery, one of the common settings is to use a system that consists of a CNN (Perception), LSTM (Temporal/Memory), and a Policy (Control) as shown in 2. The CNN-LSTM model take input observation (o_t) and outputs an embedding (z_t) that is then passed on to the policy. The policy outputs the action vector (a_t), throttle and steer. We conducted separate training for these three models solely using the data obtained from the simulator environment, followed by their seamless Zero-shot transfer into real-world robotic platforms.

This section outlines two main challenges we are concerned with in this particular Sim2Real transfer setting, along with our proposed methodologies to address them. The first challenge pertains to designing the perception model, with the objective of efficiently translating FPV images into compact intermediate representations compatible with downstream models. The second challenge involves the enhancement of the robustness and stability of the predictions during real-world testing. Solving these tasks are pivotal for effectively transferring this system to the real world.

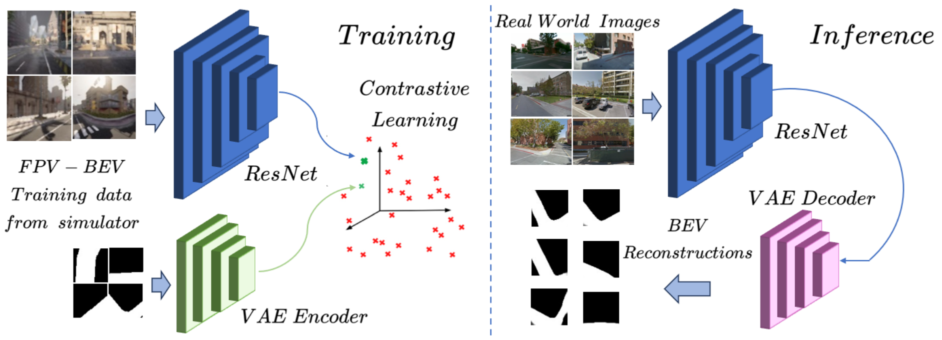

Fig. 3. Training pipeline for the perception model. During the training phase, the Resnet model is trained using FPV (First person view) images from the simulator. During the test phase, its used for inferring the embeddings of real-world RGB images. These embedding are further passed through the VAE decoder to get BEV (Birds eye view) observations.

A. *Perception model*

The perception model consists of a *ResNet-50* [5] that is tasked with processing the observation (o_t) obtained from an RGB camera, with the primary objective of comprehending the environmental context in which the robot operates. To learn consistent representations, we have opted for a design wherein the perception model compresses o_t into a consistent intermediate representation, z_t, which stays close to the corresponding BEV representation $z_t^{'}$. Our choice for BEV representations is rooted in their capacity to convey the surrounding roadmaps with minimal information redundancy. To learn the representations from the binary BEV images, we train a *Variational Autoencoder (VAE)* to encode a binary BEV image x_t into $z_t^{'} \in \mathbb{R}^{32}$. and optimize the following loss function:

$$\mathcal{L}_{VAE} = \sum_{i=0}^{B} -(y_i \cdot log(x_i) + (1-y_i) \cdot log(1-x_i)) \\ + \beta \cdot KL(\mathcal{N}(\mu_i, \sigma_i^2) \mid\mid \mathcal{N}(0,1))) \tag{1}$$

In the above loss function KL divergence is the *Kullback Leibler divergence*, y is the ground truth for reconstruction and B is the batch size. Using this loss function, the VAE Encoder will learn to embed the BEV observations x_i into a smooth Gaussian manifold that allows 2 BEV observations that are very similar, for example 2 straight roads, but a have slight variation in the angle to be closer, than a straight road and an intersection. These are the BEV embeddings the corresponding RGB images needs to be close with.

When training the perception model, we focus on 3 main principles. Firstly, irrespective of whether o_t originates from a simulator or the real-world environment, the output vector of the ResNet-50 should always be consistent by being close to the corresponding BEV vector. Secondly, BEV images must be represented in a continuous latent space that has smooth transitions to similar BEV images. Finally, the perception model (ResNet-50) must operate irrespective of any other decoder, i.e. the representations estimated by the encoder must be sufficient for performing the downstream task efficiently, Moreover, this would also allow for unsupervised training/fine-tuning of the ResNet-50 using real-world RGB sequences, which we leave for the future work.

To leverage the extensive prior knowledge embedded in a pre-trained model, we opt to train the ResNet-50 after initializing with ImageNet pre-trained weights on a large-scale dataset containing FPV-BEV image pairs captured in the simulator. To achieve the FPV-BEV translation, we align the output vector $z \in \mathbb{R}^{32}$ from the ResNet-50 with the corresponding BEV latent vector z' through *Contrastive Learning* (Fig 3). We optimize the model parameters with the cosine similarity-based contrastive loss for image encoding.

$$\begin{aligned} \mathcal{L}_{BEV}^{i} &= -\log \frac{\exp(z_i \cdot z_i'/\tau)}{\sum_{j=0}^{N} \exp(z_i \cdot z_j'/\tau)} \\ \mathcal{L}_{FPV}^{i} &= -\log \frac{\exp(z_i' \cdot z_i/\tau)}{\sum_{j=0}^{N} \exp(z_i' \cdot z_j/\tau)} \\ \mathcal{L}_{contrastive} &= \sum_{i=0}^{N} (\mathcal{L}_{BEV}^{i} + \mathcal{L}_{FPV}^{i})/2 \end{aligned} \tag{2}$$

where τ is a temperature hyper-parameter, and N denotes the training batch size. Apart from the cosine similarity-based contrastive loss, we also attempt to use the Mean Square Error (MSE) loss function:

$$\mathcal{L}_{contrastive} = \|z - z'\|_2 \tag{3}$$

B. *Temporal model with Robustness modules*

To enhance the robustness of the perception model and transfer it to the real world setting, we implemented an additional model in the pipeline. Fig. 5 shows our proposed method of robustness enhancement. This involves the integration of an LSTM, functioning as a Memory model. The LSTM was trained on sequences $\{\langle o_j, a_j \rangle\}_{j=0}^{j=T}$ gathered from sequences $\{\mathcal{T}_0, \mathcal{T}_1, .., \mathcal{T}_n\}$ in the simulator. The primary outcome of this Memory model is to effectively infuse historical context $\{\langle z_j, a_j \rangle\}_{j=0}^{j=T}$ into the prediction of $\hat{z}_t$, which forms a candidate of z_t, and enhancing the robustness of the perception module when confronted with the unseen real-world data. To model the uncertainty in future states, we add an *Mixture Density Network (MDN)* on the top of

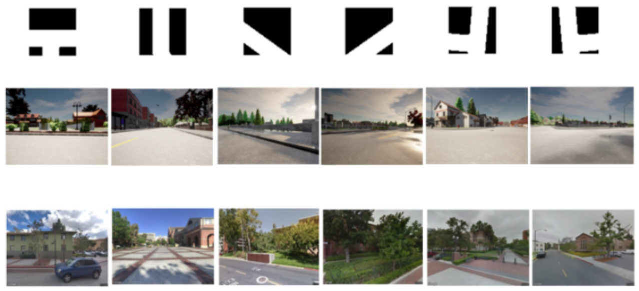

	Class#1	Class#2	Class#3	Class#4	Class#5	Class#6
Simulation Dataset	31	33	29	31	34	22
Baseline	58.1	75.8	69.0	**96.8**	29.4	68.2
Ours (Consine Similarity)	**96.8**	84.9	75.9	**96.8**	76.5	77.3
Ours (MSE)	90.3	**93.9**	**82.8**	90.3	**82.4**	**81.8**
Real-World Dataset	37	103	32	37	39	37
Baseline	47.0	43.8	54.8	91.4	9.3	31.8
Ours (Consine Similarity)	**91.9**	65.0	53.1	83.8	**35.9**	48.6
Ours (MSE)	89.2	**69.9**	**59.4**	**91.9**	**35.9**	**56.8**

Fig. 4. **Evaluation on the Validation dataset.** Left: We constructed two 6-class validation datasets: one from the simulator (second row) and another from street-view data (third row). The first row depicts the Bird's eye view (BEV) of the corresponding RGB images, which forms the basis for each class. Right: We compared our two contrastive learning approaches (MSE-based and Cosine similarity-based) against a 6-class CNN classifier. Our methods outperformed the baseline on both the unseen simulation dataset and the real-world validation dataset as shown above.

LSTM output layer. The above pipeline can be formulated as:

$$\hat{z}_t \sim P(\hat{z}_t \mid a_{t-1}, \hat{z}_{t-1}, h_{t-1}) \tag{4}$$

where $a_{t-1}, \hat{z}_{t-1}, h_{t-1}$ respectively denotes action, state prediction at the previous timestep, and historical hidden state at the time step $t-1$. $\hat{z}_t$ is the latent representation that is given as an input to the policy. Note that in the above equation, w We optimize M with the below loss function:

$$\mathcal{L}_M = -\frac{1}{T}\sum_{t=1}^{T}\log(\sum_{j=1}^{K}\theta \cdot \mathcal{N}(z_t|\mu_j, \sigma_j)) \tag{5}$$

where $\{T, K, \theta_j, \mathcal{N}(z_t|\mu_j, \sigma_j)\}$ is, respectively, the training batch size, number of Gaussian models, Gaussian mixture weights with the constraint $\sum_{j=1}^{K}\theta_j = 1$, and the probability of ground truth at time step t conditioned on predicted mean μ_j and standard variance σ_j for Gaussian model j.

Nonetheless, it is noteworthy that z_t, that is obtained from the ResNet-50 may slightly distract from the latent distribution of BEV images when the perception model is applied to real-world observations o_t, potentially impacting the performance of the LSTM and the policy. To mitigate this concern, we collected a dataset $\mathcal{S}$ comprising of the latent vectors s of 1439 BEV images which we define as the *BEV anchors*. In practice, upon obtaining the output vector z_t from the ResNet-50, we measure its proximity to each $s \in \mathcal{S}$, subsequently identifying the closest match. We replace z_t with the identified anchor embedding $\bar{z}_t$, ensuring that both the LSTM and the policy consistently uses the pre-defined BEV data distribution. We pass $\bar{z}_t$ as an input to the LSTM, along with the previous action a_{t-1} to get the output $\hat{z}_{t+1}$. Again, we find the closest match $\hat{s}_t \in S$ for $\hat{z}_t$. We call this module *Anchor State Checking (ASC)*:

$$\bar{z} = \arg\min_{s\in S} \|z - s\| \tag{6}$$

We also utilize the LSTM model for rejecting erroneous predictions by the ResNet-50, further enhancing the system's robustness against noise. If the processed prediction $\bar{z}_t$ from the perception model is estimated with confidence score τ_t, obtained from either cosine-similarity or MSE, below a predefined threshold ρ, we deliberately discard $\bar{z}_t$ and opt for $\hat{z}_t$. In such instances, we resort to the output of the LSTM at the previous time-step. This module is known as *Temporal State Checking (TSC)*:

$$\hat{z}_t = \begin{cases} \bar{z}_t, & \tau_t \geq \rho, \\ \hat{z}_{t-1}, & \tau_t < \rho. \end{cases} \tag{7}$$

Apart from adding robustness to the system using TSC, the utilization of the Memory model also serves as the crucial purpose of performing interpolation for the robots state in instances where actual observations o_t are delayed. This ensures the continuity and reliability of the entire system. There is often a notable discrepancy in the update frequencies between control signals and camera frames. Typically, control signals exhibit a significantly higher update rate compared to the incoming stream of camera frames. In some other cases, Large pretrained perception models tend to slow-down estimating the embedding from the observation.

C. *Control model*

To speedup RL for the control model, we intentionally allocate the majority of challenges to other components in the pipeline. Consequently, the training of our policy becomes a relatively straightforward endeavour. We accomplished this by training a policy employing the PPO algorithm [15]. The design of the reward function is rooted in proportionality to the number of waypoints the robot achieves to the designated goal point. In each timestep, the policy receives the current embedding of the observation z_t concatenated with the directional vector pointing towards the waypoint tasked with producing a pair of (Throttle, Steer) values.

IV. Experimental platform and setup

We collected the train dataset from the CARLA simulator to train both the Perception and the Memory model. Along with that, we also collected the validation and the test datasets from 2 different real-world sources. Following are the details on the collected datasets.

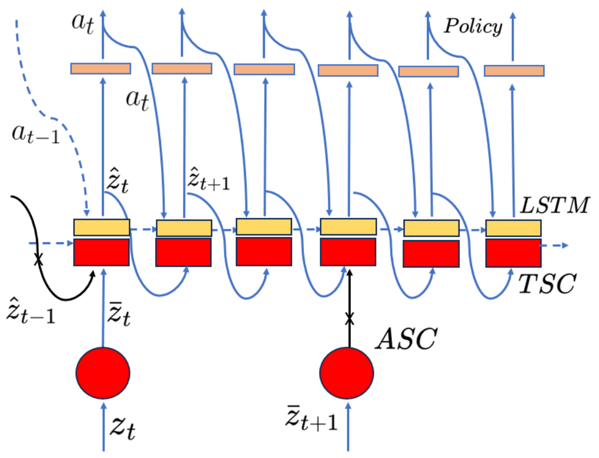

Fig. 5. **Robustness Enhancement.** *TSC* (in Red) only takes input from the representation z_t when it comes with a high confidence score. Otherwise, it takes the previous prediction by the LSTM $\hat{z}_{t-1}$ as interpolation. *ASC* improves the representation of the incoming observation by making it in-domain.

A. Data collection

1) Train dataset from CARLA simulator: Within the CARLA simulator, we have access to the global waypoints various trajectories. We added multi-camera system on the robot to obtain the data. To allow some uncertainty, we randomly sampled a range of different orientations and locations. Leveraging this setup, we facilitated the generation of a large dataset of FPV-BEV images. We augmented the simulator's realism by introducing weather randomization and non-player traffic into the simulated environment.

2) Validation dataset from Google Street View: Using the Google Street View API, we obtained all the panoramic images from various locations on the USC campus. The panoramic images were segmented with a Horizontal Field of View (FoV) of 90 degrees and are manually segregated into different 6 different classes as shown in 4. The validation dataset does not have any temporal sequencing and is primarily focused on having a broader data distribution. Due to these reasons, this dataset becomes an optimal choice for evaluating the perception model.

3) Test dataset from Beobotv3: To evaluate the quality of representations estimated by the entire system, we record a video sequence using a mobile robot. More precisely, we recorded a set of 5 *ROS Bag* sequences at different locations of the USC campus. Later, we labelled all the frames in a *ROS Bag* sequence, similar to the above paragraph. However, unlike the validation set, the test dataset has temporal continuity, which would help us to judge the system better.

B. Experimental platform

1) Scoomatic in CARLA: The CARLA simulator had been primarily tailored to self-driving applications, with a specific focus on synchronous-drive vehicles. Since all the vehicles in CARLA uses *Ackermann steering*, we further developed an existing differential drive setup using *Schoomatic* [10] and upgraded the CARLA simulator. We

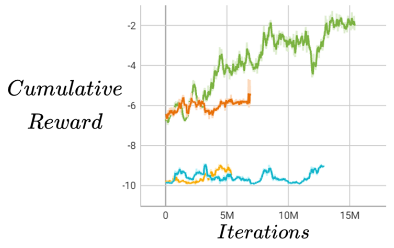

Fig. 6. **RL experiments using BEV representations**. We notice that the BEV representations enable the agent to learn faster when the waypoint threshold is higher. Green and orange correspond to waypoint threshold of 5m, resolution of 1. Blue and Yellow corresponds to waypoint threshold of 1m, resolution of 1.

find this necessary because our real-world hardware system is based on differential-drive and to enable seamless transfer without any fine-tuning, both the control systems need to have similar dynamics. Consequently, it exhibited a conspicuous deficiency in accommodating differential-drive agents. In response to this limitation, Luttkus [10] designed a scheme for the integration of a differential-drive robot into the CARLA environment. Building upon their work, we undertook the development of a dedicated simulator catering to differential-drive robots, subsequently migrating it into the newly introduced CARLA *v0.9.13*.

Our enhancements extended beyond mere implementation, including improvements to the stability of motion through the fine-tuning of its physical configuration. Additionally, we implemented a sensor designed to respond to collisions with curbs, in order to keep the robot running on roads. To ensure accessibility and ease of utilization, we have thoughtfully encapsulated the simulator within a readily deployable Docker image, which is shared for public use [1].

2) Beobotv3: For evaluating Zero-shot Sim2Real transfer, we built a hardware apparatus which is a *Non-Holonomic*, *Differential-drive* robot (*Beobotv3*) for the task of visual navigation. Our system is implemented using the *ROS (Robotic Operating System)* middleware and uses a *Coral EdgeTPU*, which is an *ASIC* chip designed to run CNN models for edge computing for all the compute. We used this particularly to run the forward inference of the ResNet-50 through a *ROS* nodes. The models are trained using the *PyTorch* framework and are integrated with the *ROS* API for inference. We integrated the *RLlib* [8] framework with *Pytorch* and CARLA to train the policy using RL.

C. Codebase for the system

As part of our open-source framework, we are realising 3 repositories, that allow users to integrate our models and system into their framework. Following are the brief outlines for each of them:

1) Model pretraining: The code pertaining to this repository allows the users to train CNN and LSTM parts of our

[1] `https://hub.docker.com/repository/docker/klekkala/carla_schoomatic`

	Class#1				Class#2				Class#3				Class#4				Class#5				Class#6			
	#	ACC	MSE	CE	#	ACC	MSE	CE	#	ACC	MSE	CE	#	ACC	MSE	CE	#	ACC	MSE	CE	#	ACC	MSE	CE
Baseline	860	**47**	0.17	2.12	1378	39	0.29	6.58	1506	**82**	0.2	3.45	1106	**81**	0.18	1.95	10	0	**0.13**	2.89	140	0	0.22	2.16
Ours (-LSTM)	860	22	**0.16**	**0.71**	1378	**81**	**0.14**	**0.45**	1506	64	**0.12**	**0.72**	1106	73	**0.13**	**0.49**	10	0	0.17	**2.19**	140	**42**	0.22	**1.49**
Baseline	657	33	0.23	1.38	1853	64	0.34	9.07	1214	**85**	0.22	4.84	326	**79**	0.39	10.47	640	19	0.46	11.25	310	21	0.4	9.06
Ours (-LSTM)	657	**52**	**0.11**	**0.80**	1853	**75**	**0.13**	**1.37**	1214	42	**0.15**	**2.16**	326	76	**0.14**	**1.62**	640	**58**	**0.35**	**6.29**	310	**28**	**0.31**	**3.93**
Baseline	1644	20	0.21	1.54	1287	49	0.31	6.36	1003	**57**	0.18	2.74	973	**94**	0.18	2.24	0	-	-	-	93	0	0.19	**1.65**
Ours (-LSTM)	1644	**22**	0.21	**0.74**	1287	**71**	**0.13**	**0.44**	1003	51	**0.09**	**0.60**	973	78	**0.12**	**0.74**	0	-	-	-	93	**15**	**0.15**	1.70
Baseline	679	33	0.21	0.13	2268	69	0.30	0.74	846	**88**	0.22	0.38	1087	**90**	0.19	0.24	63	20	0.30	0.91	57	10	0.34	0.63
Ours (-LSTM)	679	**61**	**0.10**	**0.07**	2268	**94**	**0.08**	**0.07**	846	58	**0.07**	**0.08**	1087	50	0.19	**0.06**	63	**79**	**0.11**	**0.13**	57	**45**	**0.07**	**0.16**
Ours (-LSTM)	35	3	0.30	0.50	1079	73	0.40	**0.81**	69	28	0.30	0.90	131	**91**	0.30	**0.42**	0	-	-	-	177	7	**0.40**	5.21
Ours (+LSTM)	35	**77**	**0.18**	**0.32**	1079	**78**	**0.30**	1.13	69	**81**	**0.21**	**0.77**	131	88	**0.23**	0.77	0	-	-	-	177	**50**	0.41	**1.16**
Ours (-LSTM)	50	44	0.17	**3.24**	1511	**70**	0.32	4.38	151	28	0.20	**0.60**	198	37	0.30	1.40	0	-	-	-	0	-	-	-
Ours (+LSTM)	50	**90**	**0.14**	3.89	1511	69	**0.29**	**4.21**	151	**60**	**0.19**	0.69	198	**84**	**0.18**	**0.44**	0	-	-	-	0	-	-	-
Ours (-LSTM)	253	81	**0.10**	0.70	1914	**89**	0.33	4.49	33	12	0.20	1.00	190	42.6	0.20	0.90	0	-	-	-	0	-	-	-
Ours (+LSTM)	253	**97**	0.13	**0.50**	1914	84	**0.17**	**2.40**	33	**88**	**0.17**	**0.85**	190	**88**	**0.19**	**0.70**	0	-	-	-	0	-	-	-
Ours (-LSTM)	0	-	-	-	974	83	0.32	4.42	17	29	0.26	5.22	0	-	-	-	88	90.9	0.24	4.95	78	26	0.37	9.83
Ours (+LSTM)	0	-	-	-	974	83	**0.29**	**3.99**	17	**94**	**0.19**	**3.34**	0	-	-	-	88	**92.0**	**0.23**	**4.62**	78	**59**	**0.19**	**3.42**

Fig. 7. **Experiements on the Test Dataset** Each double-row corresponds to a data sequence. We demonstrate that our approach not only attains high ACC (accuracy), but also provides a more granular BEV representation compared to the naive classifier, as indicated by the MSE (Mean Squred Error) and CE (Cross-Entropy) metrics. In the upper portion of the table, we assessed our method independently of the LSTM on an unseen temporal sequence from the simulator, contrasting it with the baseline CNN classifier. In the lower portion, we compared the performance of system with and without LSTM on a real-world data sequence. Note that dashes in the table indicate the absence of a class in the respective sequence.

system on offline trajectory sequences using our method [2].

2) RL training: With our efficient implementation of CARLA API with RLlib integration, we were able to achieve simulator training at *1000 FPS*. With the objective of enabling distributed policy training, we integrated our compiled *Scoomatic* docker-based server [3].

3) System deployment: We also release ROS based code that allows users to integrate the above modules on their real-world robot. This specifically consists of ROS based APIs to load and infer the Pytorch models using the subscribed topics [4].

Apart from the above repositories, we also release a large dataset of FPV-BEV trajectory sequences collected by the *Schoomatic* robot in the CARLA simulator along with the pre-trained models.

V. Evaluation and Results

We evaluated the performance of our ResNet-50 model using the Validation dataset and the results are shown in Table 4. The performance of our perception model on both simulation and real-world dataset are compared to the baseline, which is a 6-way ResNet-50 classifier. Our perception model identifies the closest matching class for the output embedding. The baseline is a ResNet-50 model trained on a 6-class training dataset comprising 140,213 labelled FPV images.

Following a similar approach, we used the Test dataset to evaluate the entire system. Apart from the accuracy also used Cross entropy (CE) and Mean Square error (MSE) to judge the quality of reconstructions by the LSTM model. These results are shown in Table 7. Similar to the above experiments, we also used data from the unseen Town from the CARLA simulator to asses the predictions of our system. The metrics presented in this table exhibit a slight decrease compared to Table 4. This can be attributed to the increased presence of abnormal observations and higher ambiguity between classes within the time-series data obtained from the robot, as opposed to the manually collected and labelled dataset in the validation dataset.

We then performed RL experiments by deploying the policy trained in the CARLA simulator, which can be found here 6. We used the BEV representations to learn to navigate to a goal location with different waypoint density and waypoint threshold (threshold from the waypoint to be for obtaining the reward). We noticed that BEV representations tend to learn faster when the threshold is higher.

VI. Discussion and Conclusion

In this paper we proposed a robust navigation system that is trained entirely in a simulator and frozen when deployed. We learn compact embeddings of an RGB image for Visual Navigation that are aligned with those of corresponding BEV images. By decoupling the perception model from the control model, we get an added advantage of being able to deploy the model onto a future robot with unknown dynamics. This approach also allows us to pretrain the perception and the memory model using offline datasets. Lastly, we release software and models for efficient training and deployment of the model onto a real world robot.

References

[1] Karol Arndt et al. "Meta Reinforcement Learning for Sim-to-real Domain Adaptation". In: *CoRR* abs/1909.12906 (2019). arXiv: 1909.12906. URL: http://arxiv.org/abs/1909.12906.

[2] https://github.com/klekkala/prtr_visnav
[3] https://github.com/klekkala/carla_visnav
[4] https://github.com/klekkala/deploy_visnav

[2] Mariusz Bojarski et al. "End to End Learning for Self-Driving Cars". In: *CoRR* abs/1604.07316 (2016). arXiv: 1604.07316. URL: http://arxiv.org/abs/1604.07316.

[3] Alexey Dosovitskiy et al. "CARLA: An Open Urban Driving Simulator". In: *1st Annual Conference on Robot Learning, CoRL 2017, Mountain View, California, USA, November 13-15, 2017, Proceedings*. Vol. 78. Proceedings of Machine Learning Research. PMLR, 2017, pp. 1–16. URL: http://proceedings.mlr.press/v78/dosovitskiy17a.html.

[4] David Ha and Jürgen Schmidhuber. "World Models". In: *CoRR* abs/1803.10122 (2018). arXiv: 1803.10122. URL: http://arxiv.org/abs/1803.10122.

[5] Kaiming He et al. "Deep Residual Learning for Image Recognition". In: *CoRR* abs/1512.03385 (2015). arXiv: 1512.03385. URL: http://arxiv.org/abs/1512.03385.

[6] Josip Josifovski et al. "Analysis of Randomization Effects on Sim2Real Transfer in Reinforcement Learning for Robotic Manipulation Tasks". In: *arXiv e-prints* (June 2022). DOI: 10.48550. arXiv: 2206.06282 [cs.RO].

[7] Manuel Kaspar, Juan David Munoz Osorio, and Jürgen Bock. "Sim2Real Transfer for Reinforcement Learning without Dynamics Randomization". In: *arXiv e-prints*, arXiv:2002.11635 (Feb. 2020). DOI: 10.48550. arXiv: 2002.11635 [cs.AI].

[8] Eric Liang et al. "Ray RLLib: A Composable and Scalable Reinforcement Learning Library". In: *CoRR* abs/1712.09381 (2017). arXiv: 1712.09381. URL: http://arxiv.org/abs/1712.09381.

[9] Chenyang Lu, Marinus Jacobus Gerardus van de Molengraft, and Gijs Dubbelman. "Monocular Semantic Occupancy Grid Mapping With Convolutional Variational Encoder–Decoder Networks". In: *IEEE Robotics and Automation Letters* 4.2 (2019), pp. 445–452. DOI: 10.1109/lra.2019.2891028. URL: https://doi.org/10.1109%2Flra.2019.2891028.

[10] Lennart Luttkus, Peter Krönes, and Lars Mikelsons. "Scoomatic: Simulation and Validation of a Semi-Autonomous Individual Last-Mile Vehicle". In: *Sechste IFToMM D-A-CH Konferenz 2020: 27./28. Februar 2020, Campus Technik Lienz*. Vol. 2020. Feb. 21, 2020. DOI: 10.17185/duepublico/71204. URL: https://nbn-resolving.org/urn:nbn:de:hbz:464-20200221-092453-2.

[11] Bowen Pan et al. "Cross-View Semantic Segmentation for Sensing Surroundings". In: *IEEE Robotics and Automation Letters* 5.3 (2020), pp. 4867–4873. DOI: 10.1109/lra.2020.3004325. URL: https://doi.org/10.1109%2Flra.2020.3004325.

[12] Xue Bin Peng et al. "Learning Agile Robotic Locomotion Skills by Imitating Animals". In: *CoRR* abs/2004.00784 (2020). arXiv: 2004.00784. URL: https://arxiv.org/abs/2004.00784.

[13] Lennart Reiher, Bastian Lampe, and Lutz Eckstein. "A Sim2Real Deep Learning Approach for the Transformation of Images from Multiple Vehicle-Mounted Cameras to a Semantically Segmented Image in Bird's Eye View". In: *CoRR* abs/2005.04078 (2020). arXiv: 2005.04078. URL: https://arxiv.org/abs/2005.04078.

[14] Fereshteh Sadeghi and Sergey Levine. "CAD2RL: Real Single-Image Flight Without a Single Real Image". In: *Robotics: Science and Systems XIII, Massachusetts Institute of Technology, Cambridge, Massachusetts, USA, July 12-16, 2017*. Ed. by Nancy M. Amato et al. 2017. DOI: 10.15607/RSS.2017.XIII.034. URL: http://www.roboticsproceedings.org/rss13/p34.html.

[15] John Schulman et al. "Proximal Policy Optimization Algorithms". In: *CoRR* abs/1707.06347 (2017). arXiv: 1707.06347. URL: http://arxiv.org/abs/1707.06347.

[16] Gregory J. Stein and Nicholas Roy. "GeneSIS-RT: Generating Synthetic Images for training Secondary Real-world Tasks". In: *CoRR* abs/1710.04280 (2017). arXiv: 1710.04280. URL: http://arxiv.org/abs/1710.04280.

[17] M. Tobin et al. "Domain Randomization for Transferring Deep Neural Networks from Simulation to the Real World". In: *2017 IEEE/RSJ International Conference on Intelligent Robots and Systems (IROS)*. 2017, pp. 23–30. DOI: 10.1109/IROS.2017.8202133.

[18] Joanne Truong, Sonia Chernova, and Dhruv Batra. "Bi-Directional Domain Adaptation for Sim2Real Transfer of Embodied Navigation Agents". In: *IEEE Robotics and Automation Letters* 6.2 (2021), pp. 2634–2641. DOI: 10.1109/lra.2021.3062303. URL: https://doi.org/10.1109%2Flra.2021.3062303.

[19] Jingwei Zhang et al. "VR-Goggles for Robots: Real-to-Sim Domain Adaptation for Visual Control". In: *IEEE Robotics Autom. Lett.* 4.2 (2019), pp. 1148–1155. DOI: 10.1109/LRA.2019.2894216. URL: https://doi.org/10.1109/LRA.2019.2894216.